GPPS-NA-2018-0006

INCREASING BOUNDARY LAYER STABILITY FOR VARYING DEGREES OF DIFFUSER LOADING

Dajan Mimic
Institute of Turbomachinery and Fluid Dynamics
Leibniz Universität Hannover
mimic@tfd.uni-hannover.de
Hanover, 30167, Germany

Christoph Jätz
Philipp Sauer
Florian Herbst
Institute of Turbomachinery and Fluid Dynamics
Leibniz Universität Hannover
Hanover, 30167, Germany

ABSTRACT

Increasing the pressure recovery in diffusers is an ongoing endeavour in engineering. In this paper, we analyse, based on extensive numerical simulations and experiments conducted for a wide range of half-opening angles, the effect of boundary layer stability on pressure recovery in diffusers under the influence of an unsteady rotor outflow.

We present, based on integral stage design parameters, analytically devised and empirically confirmed correlations for the quantification of additional pressure recovery in diffusers under non-uniform, unsteady inflow conditions and their sensitivity to the half-opening angle.

We demonstrate that the sensitivity of the pressure recovery to the half-opening angle is caused mainly by a change of the effective area ratio due to blockage effects and provide a simple *ansatz* to estimate the magnitude of this effect. The estimate is shown to agree with experimental and numerical data.

We define a parameter, based on the diffusion of vorticity, to quantify the processes that stabilise the boundary layer and, for the first time, present a correlation that unites a wide range of different half-opening angles.

OUVERTURE

A subsonic diffuser converts the kinetic energy of a fluid into static pressure by allowing it to expand into a greater channel cross-section. In turbomachines, diffusers are commonly applied downstream of the last compressor or turbine stage if the substantial amounts of kinetic energy of the outflow would be otherwise wasted. The application in compressors simply increases the static pressure at the outlet further. In contrast, the diffuser downstream of a turbine is used to decrease the static pressure—given a constant diffuser outlet pressure—at the diffuser inlet, i.e., turbine outlet. This yields a higher turbine pressure ratio and thus increases the turbine power output.

Because this increase in power output is achieved without additional heat input, the thermal efficiency of the turbine can be increased dramatically.

The performance of a generic diffuser can be evaluated by the dimensionless pressure recovery coefficient c_p, defined as

$$c_p = \frac{p_{\text{out}} - p_{\text{in}}}{p_{\text{tot,in}} - p_{\text{in}}}. \tag{1}$$

This coefficient is the ratio of the achieved static pressure increase to the available dynamic pressure at the diffuser inlet. For a given area ratio AR, an ideal pressure recovery coefficient $c_{p,\text{ideal}}$ can be defined assuming a non-viscous and uniform flow

$$c_{p,\text{ideal}} = 1 - \frac{\frac{1}{\text{AR}^2} + \tan^2 \alpha \left(\frac{r_{\text{in}}}{r_{\text{out}}} \right)^2}{1 + \tan^2 \alpha}, \tag{2}$$

where $\alpha = \tan^{-1}(c_\vartheta / c_m)$ is the whirl angle at diffuser inlet and $r_{\text{in}} / r_{\text{out}}$ is the ratio of the Euler radii at inlet and outlet. Therefore, the effectiveness of a diffuser ϵ can be defined as

$$\epsilon = \frac{c_p}{c_{p,\text{ideal}}}. \tag{3}$$

Due to viscous flow effects, the diffuser effectiveness will always be below unity. The predominant cause for the drop in static pressure recovery is the detachment of the boundary layer. As the flow decelerates within the diffuser, the desired static pressure gradient develops. This adverse pressure gradient is experienced to an even greater degree by the low momentum flow in the boundary layer. If the boundary layer is decelerated to a standstill, it will detach from the wall and a recirculation area will form—decreasing the effective area ratio and, thus, pressure recovery.

One possibility to reduce flow separation would be to decrease the opening angle. For the area ratio and thus pressure recovery to remain constant, the diffuser length would then

need to increase and vice versa. Diffuser length, however, is a design objective that is as important as pressure recovery, since total pressure losses in the diffuser and construction costs both scale with diffuser length. Therefore, in order to find the optimal balance between pressure recovery and boundary layer stability, empirical diffuser design charts have been devised for decades.

STABILISATION NUMBER

Empirical diffuser design charts have been developed as early as 1939 by Bardili et al. (1939) and have been further refined ever since, e.g., Sovran and Klomp (1967). They relate the geometric parameters of simple diffuser geometries to a pressure recovery coefficient. Because these charts were derived from experiments conducted with ideal inflow, additional corrections for real diffuser flows were developed and compiled, e.g., ESDU (1990). According to Vassiliev et al. (2011), inlet Mach number, total pressure distribution, flow angle, and turbulence characteristics of the inflow need to be taken into account when estimating diffuser performance.

The unsteady, inhomogeneous stage outflow entering a real diffuser adds an additional layer of complexity. Kluß et al. (2009) showed numerically for an annular diffuser, that in presence of unsteady wakes and secondary flows, the pressure recovery coefficient exceeds the predictions made by traditional design charts. This increase is the result of a stabilised boundary layer and its delayed detachment; the effective area ratio increases compared to a diffuser without an upstream stage. Subsequent experiments and additional numerical simulations conducted by Sieker and Seume (2008), Kuschel and Seume (2011), Kuschel et al. (2015), and Drechsel et al. (2015) confirmed this observation. It has been concluded that, for an efficient turbomachine diffuser design, a combined design methodology that takes the upstream stage into consideration is required.

Mimic et al. (2018) identified the velocity field induced by the tip leakage vortices in the stage as the stabilising mechanism. It was shown that elevated turbulence levels measured in the tip region are merely a symptom for the presence of these stabilising vortices. Based on a combination of deductions, simulations, and experimental data, the stage-induced increase in diffuser effectiveness with regards to design operating conditions, i.e. $\Delta\epsilon$, was correlated linearly to a novel stabilisation number

$$\Sigma \equiv \frac{\Psi f_{\text{red}}}{\Phi^2}. \qquad (4)$$

The stabilisation number comprises the dimensionless stage parameters: loading coefficient Ψ, flow coefficient Φ, and reduced frequency f_{red}, as defined in Eqn. (19) to Eqn. (21), detailed in Appendix A. The correlation for an annular diffuser with an half-opening angle of 15° is shown in Fig. 1. The increase in diffuser effectiveness is given by

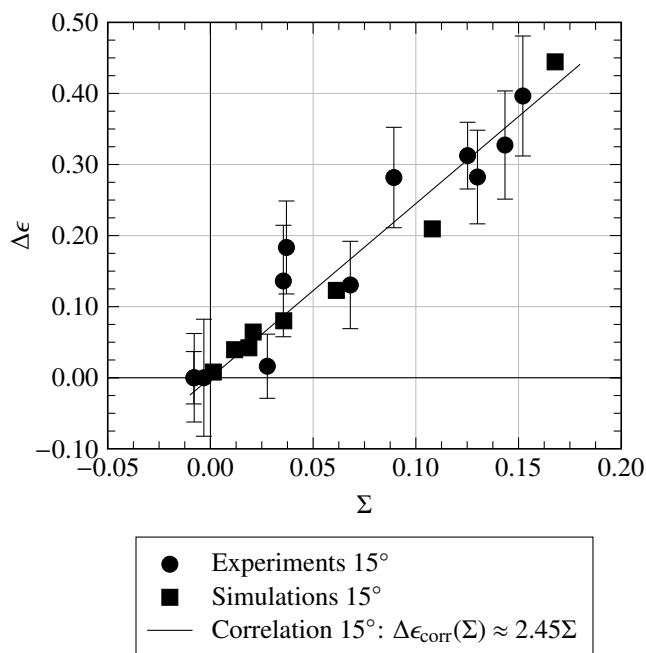$$\Delta\epsilon_{\text{corr}}(\Sigma) \approx 2.45\Sigma \qquad (5)$$

Figure 1 Increase in Diffuser Effectiveness $\Delta\epsilon$ against Stabilisation Number Σ (Mimic et al., 2018)

or, rearranged for the pressure recovery coefficient c_p,

$$c_{p,\text{corr}}(\Sigma) \approx (2.45\Sigma + \epsilon_{\text{ref}})c_{p,\text{ideal}}, \qquad (6)$$

where ϵ_{ref} is the diffuser effectiveness at reference conditions. Aerodynamically, the stabilisation number Σ captures the tip vortex characteristics depending on the stage operating point: vortex strength due to blade loading, circumferential vortex trajectory due to deflection, and spatial as well as temporal vortex packing.

The purpose of this paper is to expand the application of this correlation by investigating its sensitivity to varying degrees of diffuser loading.

PRELIMINARY DELIBERATIONS

The next step after discussing the influence of the inflow conditions into the diffuser caused by the outflow of the turbine is a look at the behaviour of different diffuser geometries. For now, we want to limit this geometric variation to the half-opening angle and, thus, the aerodynamic loading of the diffuser. A variation of the diffuser shape is left to future investigations. This paper is driven by the fundamental question below:

> How does the previously introduced correlation function of Σ to $\Delta\epsilon$ change for varying diffuser opening angles?

We expect the changes to be strongly dependent on the prevailing flow regimes (Traupel, 2001), which shall be briefly introduced in the following.

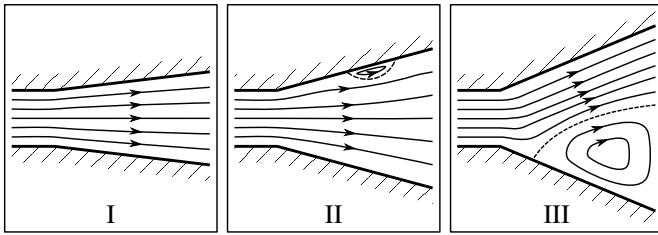I. For shallow half-opening angles, the boundary layers remain fully attached. An increased stabilisation number

Figure 2 Different Flow Regimes in Diffusers (Adapted from Traupel, 2001)

is not expected to provide considerable improvement in the diffuser flow. Some positive effect may be observed in the case of boundary layers approaching separation due to reduction of boundary layer thickness.

II. If the half-opening angle is further increased, regions of intermittent flow separation form in the diffuser. The momentum deficit in the boundary layer then strongly rises with the adversity of the pressure gradient. And where there is deficit, there is also potential benefit: accelerating the separated boundary layer presumably leads to a notable reduction in the area and extent of the flow separation and, hence, to a significant increase in pressure recovery of the diffuser by means of an increased effective area ratio.

III. In the case of even steeper half-opening angles, the diffuser flow exhibits steady separation. While an increased stabilisation number is still suspected to benefit the pressure recovery, the correlation with the half-opening angle should cease eventually, as the extent of the separation remains virtually unchanged.

In extreme cases, a fourth regime arises, where the massively separated diffuser flow forms a free jet. While this topic certainly is of academic interest, it is beyond the scope of this rather application-oriented paper.

DIFFUSER TEST RIG

Experimental investigations were performed on the low-speed axial diffuser test rig at the Institute of Turbomachinery and Fluid Dynamics. The diffuser features an inlet Mach number of 0.1 and comprises an annular and a conical section. In this paper, only the annular part is considered. Depending on the setup, the half-opening angle of the annular section is 15° or 20° with a constant area ratio of 1.78 between diffuser outlet and inlet. According to the diffuser charts of Sovran and Klomp (1967) for steady homogeneous inflow conditions, the boundary layer in both annular diffusers is prone to separation.

An upstream rotor generates unsteady inflow conditions for the diffuser, as can be observed downstream of low-pressure turbines. Two interchangeable rotating wake generators, with either 30 or 15 symmetric, twisted NACA0020 blades, allow a wide range of operating points. Because of the symmetric blades, the rotor neither performs nor extracts work under de-
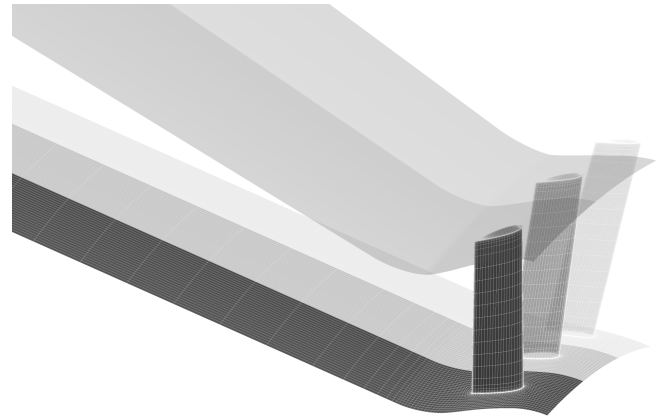

Figure 3 Computational Domain (Coarse Mesh and Multiple Rotor Pitches for Display)

sign operating conditions. However, work is extracted and tip leakage vortices develop in part-load operation, where the rotor acts as a turbine, because of changes in the incidence angle. Further details regarding the test rig and the instrumentation can be found in Kuschel et al. (2015).

NUMERICAL APPROACH

For the main practical objective of the present paper—to extend the diffuser stability correlation previously shown (see Fig. 1)—a considerable amount of data is required. For the greater part, simulations are used to gather the data, because they allow a wide range of both diffuser geometries and operating points to be considered in an efficient and flexible way. Experiments are used for the validation of critical test cases.

The non-commercial solver TRACE 8.2 (Turbomachinery Research Aerodynamics Computational Environment) from the Institute of Propulsion Technology at the German Aerospace Center (DLR) was used to carry out the simulations. To facilitate the formation of realistic vortex structures and flow separations, the k–ω-SST turbulence model by Menter (1994) was used in combination with the *Scale Adaptive Simulation (SAS)* method devised by Menter and Egorov (2010). For the same reason, inlet turbulence intensity was kept under 0.1 %. No transition modeling was employed. The stagnation point anomaly fix by Kato and Launder (1993) was used. The suitability and performance of the SST-SAS method in the resolution of the relevant flow phenomena was shown by Drechsel et al. (2016). Further details concerning the numerical setup can be found in Mimic et al. (2018).

The numerical domain consists of a rotor followed by an annular diffuser and covers one rotor pitch. For improved clarity, three rotor pitches are shown in Fig. 3. The rotor geometry matches that of the experiment. Blade counts of 25, 30, and 40 were investigated numerically. The individual diffuser variants feature half-opening angles δ of 5°, 10°, 12° and 15°.
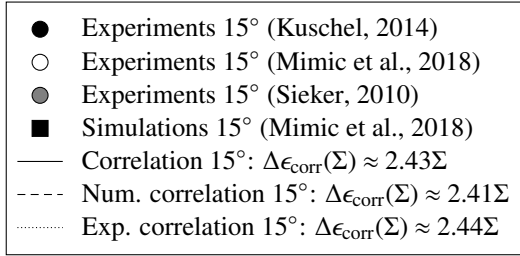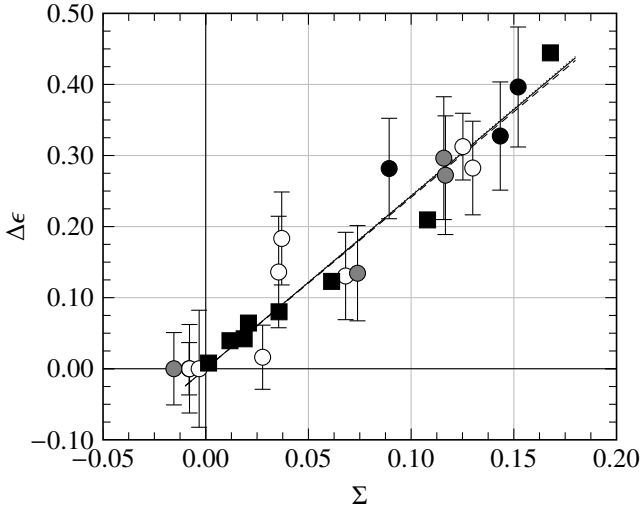
Figure 4   15° Validation

A wide range of operating points was studied for each half-opening angle. Since the operating points were attained by adjusting outlet pressure and rotor speed, as done in the experiment, the resulting Σ could not be controlled precisely. Thus, it proved difficult to achieve an even distribution of the operating points with regards to Σ.

Depending on the blade count and the diffuser half-opening angle, an individual mesh consists of 1.7 million to 2.4 million cells in total. A refined mesh was used in the tip gap region and in the vicinity of the diffuser shroud to resolve the unsteady effects in these regions, namely vortex structures at the blade tip and shroud boundary layer separation in the diffuser. Numerical convergence and stability were enhanced by the use of a coarsened mesh outlet section that dampens numerical disturbances before reaching the outlet boundary. An extensive grid convergence study with a similar grid and the SST model can be found in Drechsel et al. (2015).

EXPERIMENTAL VALIDATION

We deem important to test the underlying hypothesis of the Σ model and to explore the limitations of our approach before delving into the core of this paper. Thus, additional experimental validation, based on measurements from Sieker (2010), of the diffuser stability correlation for the 15° diffuser introduced in Eqn. (5) is provided. Moreover, since the 20° diffuser is characterised by massive flow separation and highly unsteady flow, it is an intricate test case that lends itself to this
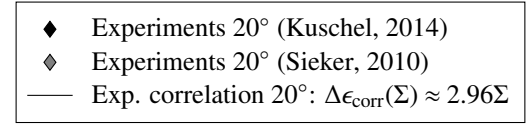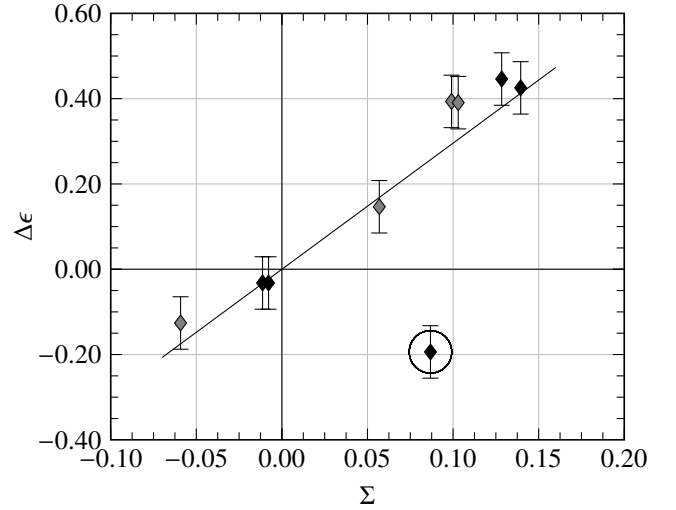
purpose of approaching the limits. In analogy to Mimic et al. (2018), a new variant of the correlation has been devised for the 20° diffuser, based on experimental data from Sieker (2010) and Kuschel (2014).

15°. As can be seen from Fig. 4, the additional data from Sieker (2010) confirms the robustness of the existing correlation for the 15° diffuser. With the added condition that $\Delta\epsilon(\Sigma = 0) = 0$, the correlation over experimental and numerical values gives

$$\Delta\epsilon_{\text{corr}}(\Sigma) = 2.4304\Sigma \approx 2.43\Sigma \quad \text{with } R^2 = 0.9235. \quad (7)$$

Additionally, Fig. 4 shows the graphs of the respective correlation functions for the numerical and experimental data sets. It is evident, that the differences between all correlation variants can be neglected.

20°. Figure 5 shows a linear correlation between the increase in diffuser effectiveness and the stabilisation number Σ for the 20° diffuser—admittedly with fewer samples. The circled point is representative for the difficulties imposed by the measurements in the 20° diffuser: in contrast to other samples near $\Sigma = 0.1$, i.e., nearly identical operating points, the pressure recovery for the outlier is not only considerably lower, but negative withal. Further investigation of the measurement data showed no distinct tip leakage vortex and leads to the conclusion that the sample was obtained via an erroneous measurement. The outlier is thus not included in the correlation for the 20° diffuser, which then gives

$$\Delta\epsilon_{\text{corr}}(\Sigma) = 2.9567\Sigma \approx 2.96\Sigma \quad \text{with } R^2 = 0.9638 \quad (8)$$

if, again, the condition that $\Delta\epsilon(\Sigma = 0) = 0$ is imposed. The result is shown in Fig. 5. Because no data were available
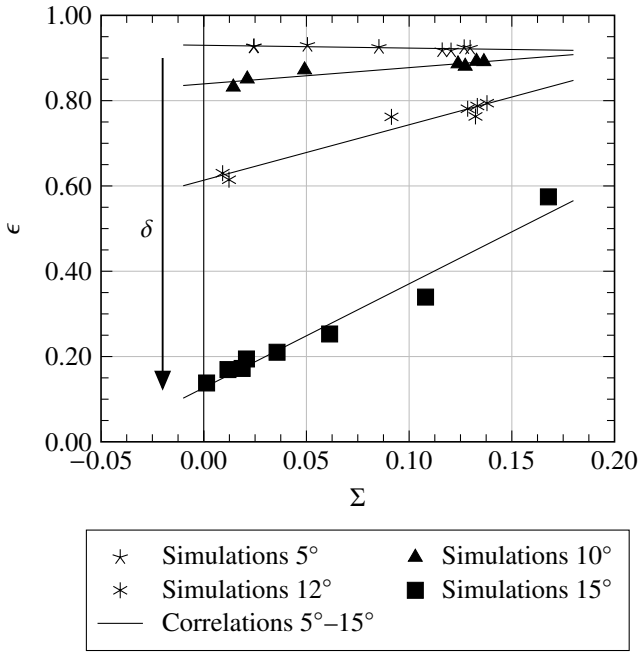

Figure 5   20° Validation

Figure 6   Correlations for Numerical Data

at the aerodynamic design point of the rotor as a reference for the 20° diffuser, ϵ was firstly correlated against Σ for the individual data sets. Then the ϵ-intercept of each correlation was used as the respective reference in order to obtain $\Delta\epsilon$. Notably, there are no simulations presented for the 20° diffuser. This is due to extremely slow convergence rates in this massively separated flow regime. Eventual results will be discussed in subsequent publications.

The results show an excellent validity of the Σ model for the 15° diffuser and the 20° diffuser. The slow convergence rates encountered indicate that steeper opening angles may require a different numerical approach. We are confident that the predictive value of the correlation method and the numerical model is appropriate for the following investigation of half-opening angles below 15°.

EXPANDING THE CORRELATION

The correlation is extended for the diffuser half-opening angles 5°, 10°, 12° using numerical data, and for the 20° diffuser using experimental data. On the diffuser test rig, each annular diffuser has a fixed area ratio of 1.78. Keeping the area ratio constant and decreasing the half-opening angle for the simulations would yield increasingly long diffusers. In that case computational costs would be significantly higher. Instead, the lengths of the numerical diffuser domains were kept the same as for the experimental 15° diffuser, resulting in a decreasing area ratio. However, since the correlations presented refer to the diffuser effectiveness, which is the pressure recovery coefficient divided by the ideal pressure recovery coefficient, the dependency from the diffuser area ratio vanishes.
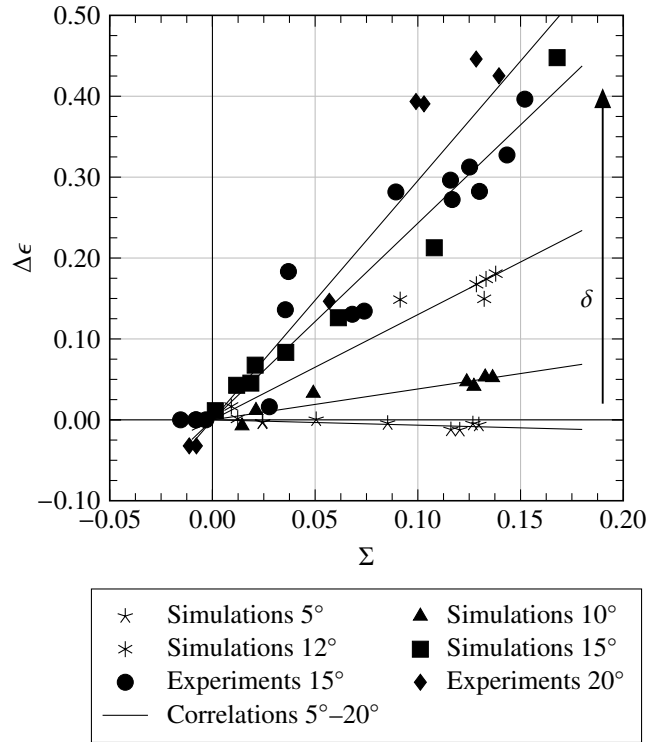

Figure 7 Correlations for Numerical and Experimental Data (Error Bars Omitted)

Figure 6 plots the diffuser effectiveness against the stabilisation number Σ. Applying the method previously used, a good linear fit is achieved for all variants investigated. It is evident that the effectiveness of an unstabilised diffuser decreases for increasing half-opening angles as can be seen at $\Sigma = 0$: for the shallowest diffuser with 5°, the effectiveness is near unity, while it plummets for the 15° diffuser. The main cause lies in the different flow regimes present at different half-opening angles: while the flow is fully attached for the 5° diffuser, growing flow separation takes place at greater half-opening angles. The respective correlation functions are listed in Appendix B.

Conversely, the slopes of the individual correlations increase as the half-opening angle increases. This becomes evident in Fig. 7, where only the increase in effectiveness $\Delta\epsilon$ is plotted against the stabilisation number.

> The beneficial effect of a given stabilisation number Σ increases for growing diffuser half-opening angles δ.

Consequently, if the value of Σ is high enough, the same diffuser effectiveness can be achieved with a steeper half-opening angle, thus, effectively reducing the required diffuser length. This newly gained insight supports our initial deliberations, which poses two further questions:

1. How does the benefit of increased Σ depend upon δ?
2. What are the fluid dynamical mechanisms involved?

We shall address these questions in the second part of this paper.

5

OPENING ANGLES AND SENSITIVITY

In order to elucidate the relationship between flow stabilisation and diffuser half-opening angle with regard to the respective flow regime, it is advantageous to choose a different graphical representation. Figure 8 depicts how the diffuser effectiveness changes with the half-opening angle for different values of Σ as the curve parameter. The sampling points for Fig. 8 have been calculated from the correlations Eqn. (26) to Eqn. (32), detailed in Appendix B. The solid line showing the behaviour for $\Sigma = 0$, i.e., a fully unstabilised diffuser. *Ex ante*, we can ascertain that the curve qualitatively matches the results that were obtained experimentally by Cochran and Kline (1958) using a flat, unstabilised diffuser—including the characteristic changes of slope somewhere between 5° and 10° half-opening angle. This roughly translates into the flow regimes described by Traupel (2001) and indicates the onset of separation.

For all values of Σ, the respective reduction in effectiveness is most pronounced for angles $\delta > 10°$, where the flow begins to separate as shown in Fig. 9. The reduction is significantly weaker for $\delta < 10°$, where the flow is fully attached and merely the boundary layer thickness is affected.

Another piece of information we can infer from Fig. 8 is that the iso-Σ curves diverge towards greater half-opening angles. This is equivalent to the slopes of the respective correlations shown in Fig. 7 and can be quantified per the sensitivity of the diffuser effectiveness to the vortex-induced boundary layer stabilisation,

$$\frac{\partial \epsilon}{\partial \Sigma}. \tag{9}$$

The general trend is a growing sensitivity towards steeper half-opening angles, which is significantly more pronounced for $\delta > 10°$. Further studies are required to determine the sensitivity for even greater half-opening angles.

In general terms, we conclude that identical turbine outflow conditions, with the same stabilising vortical structures, would yield a higher gain in diffuser effectiveness for greater half-opening angles than for smaller ones. This raises the question about the exact mechanisms that lead to this behaviour.

GEOMETRIC CONSIDERATIONS

In order to qualify the relationship of the sensitivity of Σ to the half-opening angle δ, a simple model of the annular diffuser is devised. Figure 9 shows how the flow, for an unstabilised diffuser, follows the diffuser contour until the point of separation, x_{sep}. Here, a separation develops and the streamlines are assumed to continue horizontally. This results in a smaller effective area ratio AR_{eff} compared to an ideal diffuser with no flow separation; the pressure recovery and thus diffuser effectiveness decrease. However, the point of separation moves downstream by a finite distance of Δx_Σ in the presence of tip leakage vortices characterised by the stabilisation number Σ. Correspondingly, the effective area ratio $AR_{eff,\Sigma}$ will increase
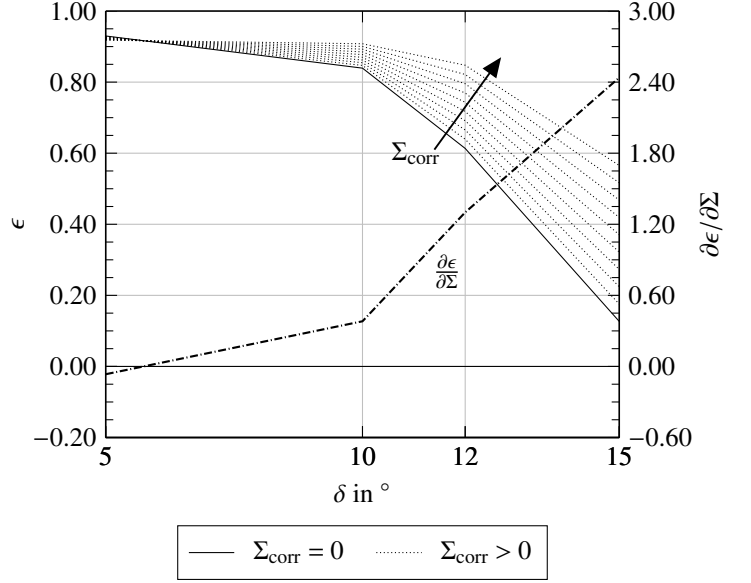

Figure 8 Correlated Diffuser Effectiveness against Half-Opening Angle for Different Stabilisation Numbers and Sensitivity of the Effectiveness

and in tandem with it the diffuser effectiveness. The respective effective outlet areas can be calculated via

$$A_{out,eff} = A_{in}$$
$$+ \pi x_{sep} \tan(\delta)(2r_{shroud,in} + x_{sep}\tan(\delta)), \text{ and} \tag{10}$$
$$A_{out,eff,\Sigma} = A_{in}$$
$$+ \pi(x_{sep} + \Delta x_\Sigma)\tan(\delta)(2r_{shroud,in} + (x_{sep} + \Delta x_\Sigma)\tan(\delta)), \tag{11}$$

where $r_{shroud,in}$ is the shroud radius at diffuser inlet. This model predicts an increase in diffuser effectiveness, if the point of separations moves downstream because of the stabilising tip vortex. This increase can be leveraged by a larger half-opening angle or an earlier point of separation at design operating conditions—the latter being often a consequence of the former.

In order to calculate the change in diffuser effectiveness due to a Σ-induced delayed separation onset, the model is calibrated for all half-opening angles investigated. The respective separation points at operating design conditions are extracted from the numerical simulations. It should be noted that because a non-viscous, uniform flow is assumed, the model is only able to predict the increase in diffuser effectiveness, but neither the absolute values for pressure recovery nor diffuser effectiveness. This could be achieved by implementing an extension to predict the total pressure losses. The groundwork for such an endeavour has been laid by Mimic et al. (2017), where the total pressure losses within an annular diffuser were correlated linearly to the stabilisation number.

The calculated change in diffuser effectiveness over the shift in separation onset is plotted in Fig. 10. It can be seen, that an increasing half-opening angle coincides with a larger
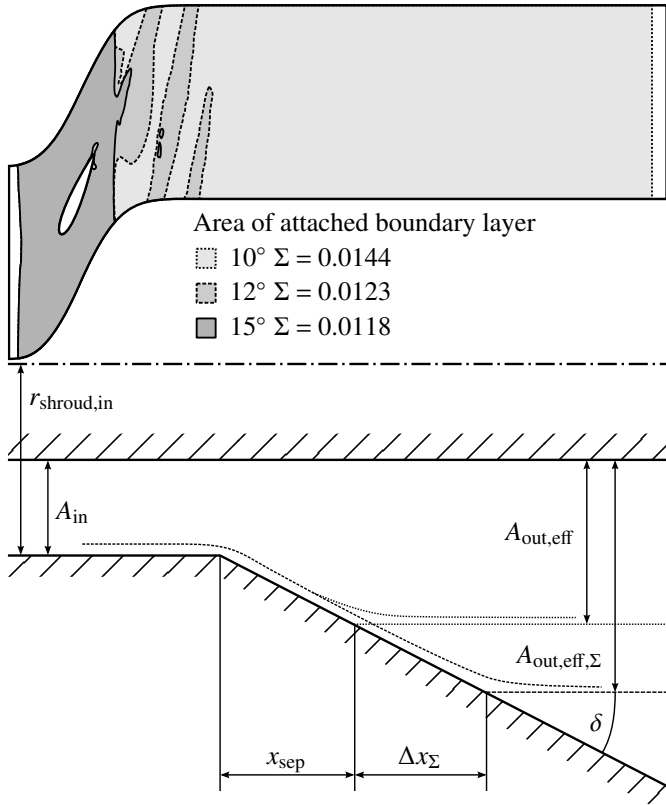
6

Figure 9 Separation Onset Shift for Different Half-Opening Angles and Resulting Changes in Effective Area Ratio

Figure 10 Estimate of Geometry-Dependent Increase in Diffuser Effectiveness (Calibrated for Numerical Data)

increase in effectiveness. Additionally, a comparison of this diagram with Fig. 7 reveals that the model not only matches the trend for each half-opening angle but also approaches the absolute values of $\Delta\epsilon$, as predicted by the correlation. This implies that the sensitivity of the diffuser effectiveness (see Eqn. 9) is dominated solely by the geometry of the diffuser and the flow field at design operating conditions. Consequently, a relationship—if it exists at all—that links the separation onset shift Δx_{sep} with the stabilisation number Σ would have to be almost independent of the half-opening angle. To gain the necessary insight into the onset-shift mechanism, we need to take a closer look at the underlying flow physics.

DIFFUSION IS THE KEY

A flow exposed to an adverse pressure gradient experiences deceleration. Some simple rearrangements of the Bernoulli equation suffice to demonstrate that this deceleration is stronger for low momentum flow. The axial momentum deficit of the boundary layer thus becomes more distinct in the presence of an adverse pressure gradient and we can deduce that the wall normal velocity gradient increases. The stabilising vortices observed add axial momentum to the boundary layer and help to mitigate the aforementioned deficit and delay or even prevent boundary layer separation (Mimic et al., 2018).
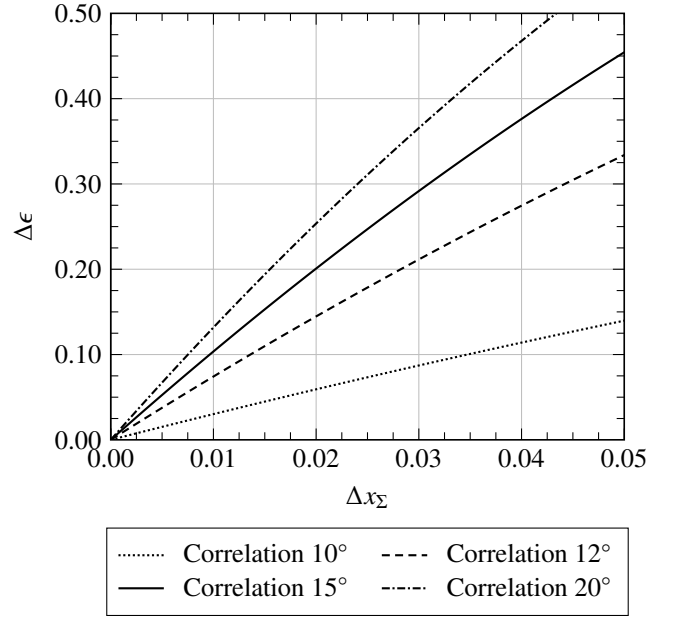
An analytical description of the exact mechanisms involved in transporting the momentum from the vortex into the boundary layer is quite cumbersome. Fortunately, the vorticity equation—which is obtained by taking the curl of the Navier–Stokes equations—represents an elegant alternative. Assuming incompressible flow, an isotropic fluid, and conservative body forces, the vorticity equation can be written as

$$\rho \frac{\partial \omega_i}{\partial t} + \rho c_j \frac{\partial \omega_i}{\partial x_j} = \rho \omega_j \frac{\partial c_i}{\partial x_j} + \mu \frac{\partial^2 \omega_i}{\partial x_j \partial x_j} \tag{12}$$

$$\text{with } \omega_i \equiv \varepsilon_{ijk} \frac{\partial c_k}{\partial x_j}. \tag{13}$$

It describes how the vorticity of a fluid parcel moving with the flow changes over time. Considering a two-dimensional, wall-bounded flow—with wall-parallel and wall-normal coordinates x_1 and x_2—and the vorticity component normal to our plane ω_3, we can further simplify the equation to

$$\rho \frac{\partial \omega_3}{\partial t} + \rho c_j \frac{\partial \omega_3}{\partial x_j} = \mu \frac{\partial^2 \omega_3}{\partial x_j \partial x_j}. \tag{14}$$

When we consider boundary layer acceleration, our sole interest lies on the wall-normal vorticity transport between vortex and boundary layer, i.e., in the x_2 direction. Consequently, we are able to reduce the above equation to a one-dimensional problem, i.e.,

$$\rho \frac{\partial \omega_3}{\partial t} + \rho c_2 \frac{\partial \omega_3}{\partial x_2} = \mu \frac{\partial^2 \omega_3}{\partial x_2 \partial x_2}. \tag{15}$$

$$\frac{\partial p}{\partial x_1} < 0 \qquad \frac{\partial p}{\partial x_1} > 0 \qquad \frac{\partial p}{\partial x_1} > 0 \qquad \frac{\partial p}{\partial x_1} > 0$$

$c_1(x_2)$

x_2

x_1

Attached flow Separated flow Superimposed vortex After vorticity diffusion

$\omega_3(x_2)$
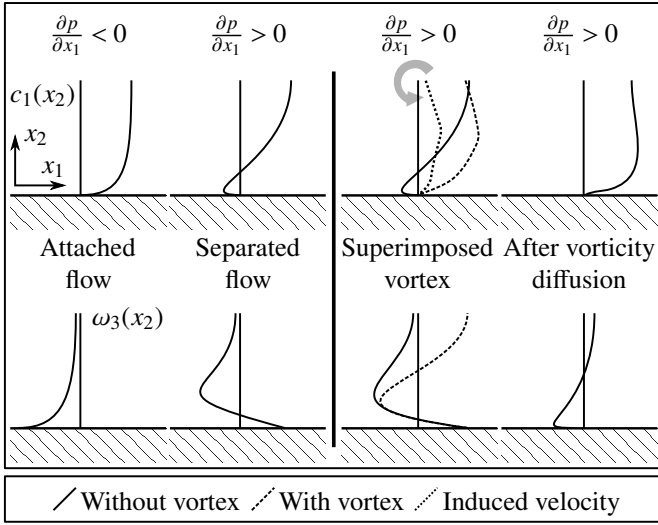
/ Without vortex ⁄ With vortex ⁄ Induced velocity

Figure 11 Velocity and Vorticity Profiles of Boundary Layer States and Stabilisation by Means of Wall-Normal Vorticity Diffusion

Using this equation, we are able to model a boundary layer at the wall and a vortex in the vicinity of the boundary layer—essentially a rudimentary version of our diffuser flow—as a wall-normal vorticity distribution. The circulatory velocity field induced by this vorticity distribution can simply be superimposed onto a wall-parallel potential velocity field, which implies that the convective transport in the x_2 direction can be neglected for our problem. The equation then gives

$$\rho \frac{\partial \omega_3}{\partial t} = \mu \frac{\partial^2 \omega_3}{\partial x_2 \partial x_2} \qquad (16)$$

and describes the one-dimensional diffusion of vorticity between vortex and boundary layer. As indicated by the left side of Fig. 11, an attached boundary layer is characterised by a negative vorticity that reaches its minimum immediately at the wall. Since the free-stream is irrotational, a flux of negative ω_3 vorticity in positive x_2 direction can be observed in this case, i.e. negative wall-normal diffusion. Contrarily, in the case of a separated flow, the vorticity profile exhibits a maximum at the wall. The wall-normal diffusion is then positive. Now, if a vortex with positive vorticity is introduced and superimposed onto the boundary layer, the near-wall flow experiences an acceleration. In terms of vorticity, the new local maximum caused by the vortex leads to a flux of positive vorticity in the negative x_2 direction, i.e., negative wall-normal diffusion. This has a positive effect on the boundary layer; depending on the relative strength of the vortex, favourable negative near-wall vorticity may be achieved. We conclude that the wall-normal diffusion of vorticity describes the main mechanism involved in boundary layer stabilisation. This implies that an influx of positive vorticity into the boundary layer is an indicator of this stabilisation process.

★ Simulations 5° ▲ Simulations 10°
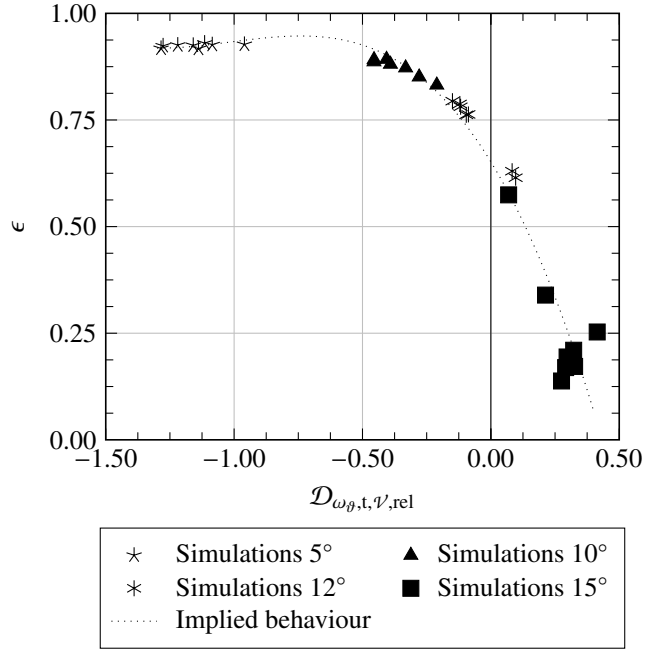✳ Simulations 12° ■ Simulations 15°
⋯ Implied behaviour

Figure 12 Correlation of Diffuser Effectiveness against Non-Dimensional Averaged Radial Diffusion of Circumferential Vorticity for Various Diffuser Half-Opening Angles from Numerical Data

To obtain an estimate for the magnitude of this effect, we analyse the volumetric average of the radial diffusion of circumferential vorticity, i.e.,

$$\mathcal{D}_{\omega_\vartheta,\mathrm{t},\mathcal{V}} \equiv \frac{1}{\mathcal{V}} \int_{\mathcal{V}} (\mu + \mu_\mathrm{t}) \frac{\partial^2 \omega_\vartheta}{\partial(-r)\partial(-r)} \, \mathrm{d}V \qquad (17)$$

$$\text{with } \omega_\vartheta \equiv \frac{\partial(-c_r)}{\partial x} - \frac{\partial c_x}{\partial(-r)}, \qquad (18)$$

where μ and μ_t are the molecular and turbulent viscosity. Thus, we are able to account for the impact of elevated turbulence levels on diffusion. It must be noted that, for the sake of simplicity, we substitute the gradient in wall-normal direction with the gradient in *negative* radial direction; the radial velocity changes sign accordingly. The inlet and outlet of the integration domain are chosen according to the measurement planes of the 15° diffuser. In radial direction, it ranges from 90% of the smallest channel height up to the diffuser shroud, so as to capture the boundary layer, the separation and the blade tip vortices, yet exclude any distracting effects that may arise at hub or mid-span and are not relevant to this paper.

Figure 12 reveals a distinct correlation between the diffuser effectiveness and the average diffusion $\mathcal{D}_{\omega_\vartheta,\mathrm{t},\mathcal{V}}$, which unites all numerically considered diffuser half-opening angles under varying inflow conditions. Consequently, the average diffusion $\mathcal{D}_{\omega_\vartheta,\mathrm{t},\mathcal{V}}$ in the shroud-near region provides a valid flow field characteristic to describe the process of boundary layer stabilisation and to predict diffuser effectiveness. Such a correlation could serve as a tool to evaluate the increase in diffuser stability,
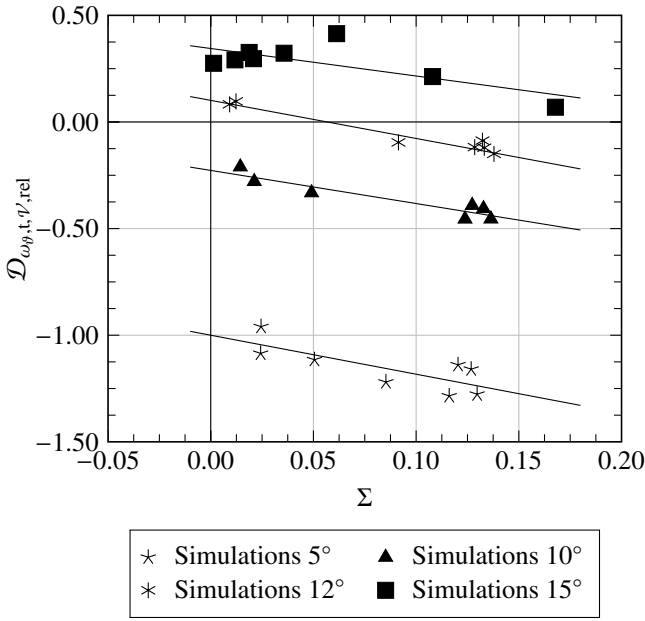
| ⋆ | Simulations 5° | ▲ | Simulations 10° |
| * | Simulations 12° | ■ | Simulations 15° |

Figure 13 Non-Dimensional Averaged Radial Diffusion of Circumferential Vorticity against Stabilisation Number for Various Half-Opening Angles

$\Sigma = 0.1328$
$\delta = 10°$

$\Sigma = 0.1379$
$\delta = 12°$

Figure 14   Decaying Circumferential Vorticity

and, thus, pressure recovery, for any given radial inflow profile. That way it would be possible to devise a generalised method that may prove essential in future combined design approaches of turbine and diffuser.

The next step in determining how the physical mechanism of boundary layer stabilisation is linked to the rotor outflow, is to regard the relationship of the average diffusion $\mathcal{D}_{\omega_\vartheta,\text{t},\mathcal{V}}$ to the stabilisation number Σ. We can infer from Fig. 13 that the sensitivity, i.e. the derivative, of the average diffusion with regards to the stabilisation number is approximately constant—even across different diffuser half-opening angles. The slightly different slopes of the respective graphs can be attributed to scattering of the samples and inaccuracies in the simplified approach towards the estimation of $\mathcal{D}_{\omega_\vartheta,\text{t},\mathcal{V}}$. This is exceptionally prominent for the 15° diffuser, which is characterised by strong, highly unsteady flow separation. Nevertheless, to make this observation more tangible, Fig. 14 shows, for a representative meridional plane, that the circumferential vorticity decay under comparable inflow conditions remains unchanged for different half-opening angles. These results allow us to conclude that the vorticity expenditure of the stabilising vortices does not depend upon geometry variations of the diffuser, as we established in the previous section, based on geometric considerations: the Σ-induced separation onset shift Δx_{sep} is independent from the diffuser half-opening angle. Any variations in sensitivity that occur, can be attributed to a change of the effective area ratio due to blockage effects.

CONCLUSIONS

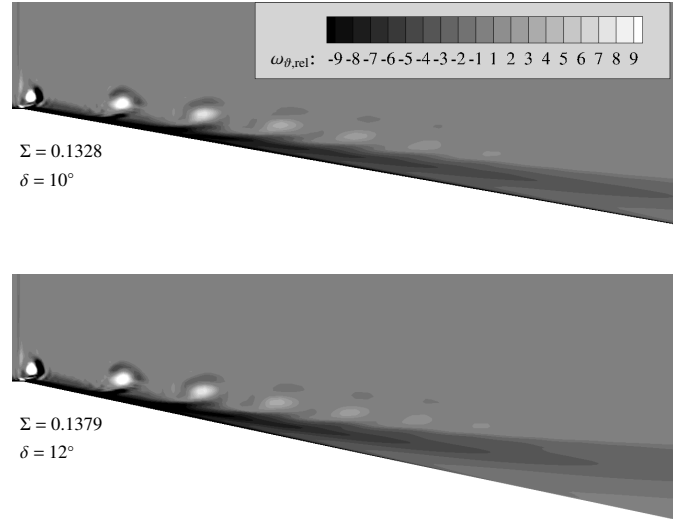In this paper, multiple advancements in the understanding of stage-to-diffuser interactions are achieved. The robustness of the diffuser stability number Σ is once again demonstrated by applying the correlation to new sets of experimental data. In addition, based on the same method and additional experimental data, a correlation is formed for an annular diffuser with an half-opening angle of 20°. Again, a linear relationship between $\Delta\epsilon$ and Σ is observed. Both results support the underlying hypothesis of the correlation: the induced velocity field of tip leakage vortices from an upstream rotor stabilises the boundary layer in an annular diffuser and increases pressure recovery.

The correlation is—by use of numerical simulations and experiment—extended further for different diffuser loadings by varying the half-opening angle from 5° to 20°. The results show that, with an increase in diffuser loading, the flow becomes more sensitive to an increase in Σ. A simple diffuser model reveals that this increased sensitivity can be attributed to a change of the effective area ratio due to blockage effects. The increase in diffuser effectiveness due separation onset shift is predicted to a high degree. The results suggest that diffusers downstream of a turbine could be designed with more aggressive half-opening angles, as those benefit the most from the stabilisation. The open question is the relationship between the stabilisation number Σ and the separation onset shift Δx_Σ.

The state of the boundary layer of a diffuser can be described by its vorticity profile while the stabilising processes can be quantified using the wall-normal vorticity diffusion $\mathcal{D}_{\omega_\vartheta,\text{t},\mathcal{V}}$. By calculating its volumetric average in the shroud-near region, it is shown that the radial diffusion is a valid flow field characteristic to describe the boundary layer stabilisation in a diffuser. Complementary to the insight that the sensitivity of the diffuser effectiveness to the stabilisation number Σ is dominated by geometric effects, it is revealed that the sensitivity of $\mathcal{D}_{\omega_\vartheta,\text{t},\mathcal{V}}$ to Σ is independent of the geometry. These insights could prove helpful in combined design approaches of turbine and diffuser. Thus, further research is deemed promising.

While the applied SST-SAS turbulence model proved to be well suited to this investigation, operating points with large flow separation, i.e., large half-opening angles, caused very slow convergence rates. Thus, it is planned to conduct additional detached eddy simulations (DES) that will extend the data field, test the hypothesis further and define its limitations. Subsequent work shall address total pressure loss correlations across various degrees of diffuser loading.

NOMENCLATURE

Symbols

AR	area ratio of the diffuser
c_i	flow velocity
c_p	pressure recovery coefficient
$\mathcal{D}$	diffusion
f_{bp}	blade passing frequency
f_{red}	reduced frequency
ℓ_c	chord length
n	blade count
N	rotational speed
p	pressure (default: static)
r	radius
R^2	coefficient of determination
t	time
u	rotational velocity
x	axial coordinate
x_i	generalised spatial coordinate
α	flow angle, swirl angle
ϵ	diffuser effectiveness
ϑ	circumferential coordinate
μ	dynamic viscosity
μ_t	turbulent eddy viscosity
ρ	density
Σ	stabilisation number
Φ, Ψ	flow coefficient, loading coefficient
ω_i	vorticity

Subscripts

I, II	rotor inlet plane, rotor exit plane
avg	average over domain
corr	correlated
in, out	diffuser inlet/outlet
ref	reference
rel	relative
sep	separation
t	turbulent quantity
tot	total quantity
i, j	generic indices

ACKNOWLEDGMENTS

Appendix A: Rotor Design Parameters

As defined by Wilson and Korakianitis (2014):

$$\Psi \equiv \frac{c_{\vartheta,\mathrm{I}} - c_{\vartheta,\mathrm{II}}}{u}, \tag{19}$$

$$\Phi \equiv \frac{c_x}{u}, \text{ and} \tag{20}$$

$$f_{red} \equiv \frac{nN\ell_c \frac{1}{60}}{c_x}. \tag{21}$$

Appendix B: Correlations

As shown in Fig. 6:

$$\epsilon_{\mathrm{corr,NUM}}(\Sigma, \delta = 5°) \approx -0.0657\Sigma + 0.9298, \tag{22}$$

$$\epsilon_{\mathrm{corr,NUM}}(\Sigma, \delta = 10°) \approx 0.3812\Sigma + 0.8393, \tag{23}$$

$$\epsilon_{\mathrm{corr,NUM}}(\Sigma, \delta = 12°) \approx 1.3006\Sigma + 0.6134, \text{ and} \tag{24}$$

$$\epsilon_{\mathrm{corr,NUM}}(\Sigma, \delta = 15°) \approx 2.438\Sigma + 0.1267. \tag{25}$$

As shown in Fig. 7:

$$\epsilon_{\mathrm{corr,NUM}}(\Sigma, \delta = 5°) \approx -0.066\Sigma + 0.9297, \tag{26}$$

$$\epsilon_{\mathrm{corr,NUM}}(\Sigma, \delta = 10°) \approx 0.3814\Sigma + 0.8399, \tag{27}$$

$$\epsilon_{\mathrm{corr,NUM}}(\Sigma, \delta = 12°) \approx 1.3006\Sigma + 0.6172, \tag{28}$$

$$\epsilon_{\mathrm{corr,NUM}}(\Sigma, \delta = 15°) \approx 2.438\Sigma + 0.1267, \tag{29}$$

$$\epsilon_{\mathrm{corr,EXP}}(\Sigma, \delta = 15°) \approx 2.41\Sigma + 0.1267, \tag{30}$$

$$\epsilon_{\mathrm{corr}}(\Sigma, \delta = 15°) \approx 2.4304\Sigma + 0.1267, \text{ and} \tag{31}$$

$$\epsilon_{\mathrm{corr,EXP}}(\Sigma, \delta = 20°) \approx 2.9567\Sigma - 0.0031. \tag{32}$$

REFERENCES

Bardili, W., Notter, O., Betz, B., and Ibel, G. (1939). "Wirkungsgrad von Diffusoren". German. In: *Bericht des Flugtechnischen Instituts an der Technischen Hochschule Stuttgart*, pp. 691–697.

Cochran, D. L. and Kline, S. J. (1958). *Use of Short Flat Vanes for Producing Efficient Wide-angle Two-dimensional Subsonic Diffusers*. NACA Technical Note. National Advisory Committee for Aeronautics.

Drechsel, B., Müller, C., Herbst, F., and Seume, J. R. (2015). "Influence of Turbulent Flow Characteristics and Coherent Vortices on the Pressure Recovery of Annular Diffusers Part B: Scale-Resolving Simulations". In: *Proc. ASME. 56635*. Vol. 2A. Paper No. GT2015-42477, V02AT38A010:1–13. DOI: 10.1115/GT2015-42477.

Drechsel, B., Seume, J. R., and Herbst, F. (2016). "On the Numerical Prediction of the Influence of Tip Flow on Diffuser Stability". In: *International Journal of Gas Turbine, Propulsion and Power Systems (JGPP)* 8.3, pp. 29–38.

ESDU (1990). *Introduction to design and performance data for diffusers*. No. 76027. London, UK: Engineering Sciences Data Unit. ISBN: 9780856791642.

Kato, M. and Launder, B. E. (1993). "The Modelling of Turbulent Flow Around Stationary and Vibrating Square Cylinders". In: *9th Symposium on Turbulent Shear Flows*, pp. 10.4.1–10.4.6.

Kluß, D., Stoff, H., and Wiedermann, A. (2009). "Effect of Wakes and Secondary Flow on Re-attachment of Turbine Exit Annular Diffuser Flow". In: *ASME J. Turbomach.* 131.4, 041012:1–12. DOI: 10.1115/1.3070577.

Kuschel, M. (2014). "Einfluss von Sekundärströmungen auf den Druckrückgewinn in Axialdiffusoren". Ph.D. Thesis. Germany: Leibniz Universität Hannover.

Kuschel, M., Drechsel, B., Kluß, D., and Seume, J. R. (2015). "Influence of Turbulent Flow Characteristics and Coherent Vortices on the Pressure Recovery of Annular Diffusers Part A: Experimental Results". In: *Proc. ASME. 56635.* Vol. 2A. Paper No. GT2015-42476, V02AT38A009:1–13. DOI: 10.1115/GT2015-42476.

Kuschel, M. and Seume, J. R. (2011). "Influence of Unsteady Turbine Flow on the Performance of an Exhaust Diffuser". In: *Proc. ASME. 54679.* Vol. 7. Paper No. GT2011-45673, pp. 1551–1561. DOI: 10.1115/GT2011-45673.

Menter, F. R. (1994). "Two-Equation Eddy-Viscosity Turbulence Models for Engineering Applications". In: *AIAA Journal* 32.8, pp. 1598–1605. DOI: 10.2514/3.12149.

Menter, F. R. and Egorov, Y (2010). "The Scale-Adaptive Simulation Method for Unsteady Turbulent Flow Predictions. Part 1: Theory and Model Description". In: *Flow Turbulence Combust.* 85.1, pp. 113–138. DOI: 10.1007/s10494-010-9264-5.

Mimic, D., Drechsel, B., and Herbst, F. (2018). "Correlation between Pressure Recovery of Highly Loaded Annular Diffusers and Integral Stage Design Parameters". In: *ASME J. Turbomach.* In press. DOI: 10.1115/1.4039821.

Mimic, D., Jätz, C., and Herbst, F. (2017). "Correlation between Total Pressure Losses of Highly Loaded Annular Diffusers and Integral Stage Design Parameters". In: *Proceedings of GPP Forum: Shanghai 2017.* Paper No. GPPS-2017-0063. Shanghai, China.

Sieker, O. (2010). "Einfluss von Drall und Nachlaufdellen auf das Strömungsverhalten und den Druckrückgewinn in axialen Turbinenaustrittsdiffusoren". Ph.D. Thesis. Germany: Leibniz Universität Hannover.

Sieker, O. and Seume, J. R. (2008). "Influence of rotating wakes on separation in turbine exhaust diffusers". In: *J. Therm. Sci.* 17.1, pp. 42–49. DOI: 10.1007/s11630-008-0042-9.

Sovran, G. and Klomp, D. (1967). "Experimentally determined Optimum Geometries for Rectilinear Diffusers with Rectangular Conical or Annular Cross-Section". In: *Fluid Mech. Int. Flow*, pp. 270–319.

Traupel, W. (2001). *Thermische Turbomaschinen*. Springer-Verlag.

Vassiliev, V., Irmisch, S., Abdel-Wahab, S., and Granovskiy, A. (2011). "Impact of the Inflow Conditions on the Heavy-Duty Gas Turbine Exhaust Diffuser Performance". In: *ASME J. Turbomach.* 134.4, 041018:1–9. DOI: 10.1115/1.4003714.

Wilson, D. G. and Korakianitis, T. (2014). *The Design of High-Efficiency Turbomachinery and Gas Turbines*. MIT Press. ISBN: 9780262526685.